J. Appl. Comput. Mech., 11(3) (2025) 742-753
DOI: 10.22055/jacm.2024.47775.4785

ISSN: 2383-4536
jacm.scu.ac.ir

Shahid Chamran University of Ahvaz

Journal of Applied and Computational Mechanics

Research Paper

Numerical Assessment of Solar System Including Trombe Wall and Photovoltaic Module

E. Azizi, H. Safarzadeh

Department of Mechanical Engineering, Razi University, Kermanshah, Iran

Received August 16 2024; Revised October 18 2024; Accepted for publication October 28 2024.
Corresponding author: E. Azizi (elazizi509@gmail.com), H. Safarzadeh (hsafarzadeh@razi.ac.ir)

Abstract. In current study, a model is developed for a one-story building with specific dimensions, integrating photovoltaic panels and Trombe walls to generate electricity and reduce energy consumption. The location chosen for the study is Kermanshah, using real climate data from the Meteonorm software to ensure accuracy. The proposed system is constructed using the TRNSYS dynamic simulation program, supplemented by a plugin for simulating the building's physical properties. The goal is to analyze the power output of the panels, their energy efficiency, airflow velocity through the channel, and the building's exergy change resulting from the addition of the Trombe wall. Additionally, a parametric analysis is scrutinized over the previous year to examine the efficacy of duct depth on various functional aspects of the system. The findings reveal that the solar panels reach their peak power generation during July and August, with a highest output of 207 kW. The exergy efficiency of the panels consistently exceeds their energy efficiency across different months, reaching up to 20% and 22%, respectively. Moreover, incorporating a Trombe wall leads to a 3% decrement in the building's cooling and heating load, with exergy efficiency peaking at a wall depth of 10 (cm). Increasing the channel depth is found to decrease the heating requirement while improving airflow through the channel.

Keywords: Trombe wall; Photovoltaic; Energy analysis; Exergy analysis; Solar energy.

1. Introduction

The world's power generation sector has seen significant changes recently due to continual industry advancements, innovative uses of energy resources, and continuous economic expansion. In the meantime, a sizable portion of power, cooling, and heating has come from renewable energy sources. The massive and continuous augmentation in energy demand that is reducing the use of traditional energy sources is one of the main issues [1]. The availability of traditional energy sources is limited, and concerns about the environment and fuel prices have grown significantly [2]. Due to its potential to reduce global warming and produce cleaner power, renewable energy (RE) has attracted a lot of attention [3]. Today's residential demands, in particular, may be partially satisfied by RE sources, particularly solar energy. One of the most researched subjects at the moment is the combination of solar cells with Trombe walls; this system is called a photovoltaic/Trombe wall (PV/TW). Homes can be heated, water can be heated, and energy can be produced all at once using a PV/TW system [4]. The building industry consumes the most energy globally, and our nation is not an exception to this norm; the building sector accounts for more than 40% of the nation's energy consumption [5]. Moreover, the building industry uses between 30 and 40 percent of global energy resources [6]. Up to 30% less energy can be used in buildings when Trombe walls are used [7]. Thermal or storage walls are other names for Trombe walls (TW) [8]. It is constructed from substantial concrete blocks, has a dark external paint job, and is coated with glass. This type of technology uses passive solar heating [9]. The south wall of any room or structure typically incorporates TW [10]. A Trombe wall contains one or two layers of glass on the outside, is 0.2–0.4 m thick, and is painted black or coated with another heat-absorbing substance [11]. As TW may provide both natural ventilation and heating, it is one of the approaches used in sustainable construction [12]. Chen et al. [13] scrutinized the free movement in the TW system of a building located in the northern cold climate region of China. In this research, the flow regime changes from calm to turbulent, while during free movement, the turbulent flow covers the mass wall's height. In this experiment, the temperature results were collected, averaged by the computer every 10 minutes, and then displayed. Based on the obtained results, the influencing factors on the room's air temperature are: the solar radiation's intensity (I), the temperature of the inner surface of the Trombe wall (Twi), the enthalpy of the air passing through the upper vent of the wall, and the temperature of the outside environment (Ta). Chen et al.'s [14] experimental study examined how the TW affects the temperature of room air. In this research, an experimental room and a main room are placed together. The test room includes the TW system, and the main room is without the TW system. The study's findings indicated that the test room's air temperature is three to five degrees Celsius warmer than the main room's in the building's southern section. The test room's temperature fluctuated more than the main room's because of the TW, but in general,

Published online: November 02 2024

according to the graphs and results, the Trombe wall provided suitable conditions for the space inside the room. The thermal behavior of composite TWs was scrutinized by Shen et al. [15]. The outputs indicated that during the day, the fluctuations of the values obtained for the composite wall are lower than the fluctuations of the normal wall; moreover, the composite wall performs better than the typical wall, particularly on gloomy and chilly days. The heat transport in a composite wall solar chamber with a porous absorber was quantitatively studied by Chen et al. [16]. The outcomes showed that the separated state has a greater range of temperature changes than the direct contact state. This research investigated two types of absorbers. One of the absorbers is quartz, and the other is marble. The quartz absorber creates a higher temperature in the room than marble. Nwachukwu and Okonkwo [17] investigated the effect of an absorber plate with a variable distance from the wall on the performance of the TW system in the solar chamber. According to the findings, by raising the thermal plate's absorption capacity, the heat absorbed and transferred along the TW improved. Using TRNSYS software, Irshad et al. [18] produced a modeling approach of a test room with a PV/TW unit. Different kinds of glass cover and air mass flow rates were found to have an impact on the PV/TW system's efficiency. The findings show that while the PV efficiency rose, the cooling load and room temperature were significantly reduced in the double-walled PV/TW unit filled with argon gas. Algburi et al. [19] investigated the performance of a PV/TW system by building an experimental model and researching the impacts of phase transition materials, reflecting mirrors, and cooling techniques. They illustrated that the solar panel's productivity and wattage rose when DC fans and a heat exchanger were used to cool it. This resulted in a drop in the panel's temperature and less energy loss. Additionally, by absorbing heat, the phase change material's use assisted in cooling the solar panel. As it releases heat into the area where it is positioned, it also helps to increase the building's heating in the afternoon. Electrical energy increased as a result of increased solar radiation, which was facilitated by the use of reflecting mirrors. Combining these various layouts yielded the maximum electrical and thermal efficiency (10.42% and 78.59%, respectively). Using TRNSYS software to model the new TW with multi-energy nanogrid, Kalair et al. [20] examined the energy performance. The simple payback period ranged from 1.1 to 4.76 years, depending on the kind of structure, build, and energy costs. In the summer, the thermal wall could hold up to 55 °C of hot air, and in the winter, 40 °C. With solar collectors, the yearly thermal energy production was 2828 kW, and the TW produced 8677 kWh of energy. The proportion of yearly comfort level (CLP) has increased from 49% to 87.5%. The architecture could fulfill 45% of the need for energy during peak winters; the remaining 55% of energy was imported from the grid. On average, on subtropical days, the system could cover 85–90% of the thermal demands. Sheikholeslami and Al-Hussein [21, 22] investigated a new configuration of the Trombe wall using ANSYS FLUENT software. They proposed adding a new layer to the classic Trombe wall and offered various fin configurations to improve its performance.

The innovation of the present research lies in its comprehensive exploration of the integration of photovoltaic panels and Trombe walls to optimize energy efficiency in building structures. While previous research has often focused on individual energy-saving techniques, such as photovoltaic systems or passive heating methods like Trombe walls, few studies have delved into their combined utilization within a single building system. By combining these technologies, the study addresses a notable research gap in the field of sustainable building design. Additionally, the investigation conducts a detailed parametric examination to evaluate the impact of channel depth on various functional aspects of the system. This nuanced approach adds a new dimension to existing research by providing insights into the optimal design parameters for maximizing energy efficiency and reducing heating and cooling loads in buildings. Through this innovative approach, the study contributes to advancing the understanding of integrated renewable energy systems and their potential to revolutionize the way buildings are designed and operated for enhanced sustainability.

2. Description of Model

The PV/TW system takes into account the optimal technology and utilizes solar energy to generate power and heat and cool different temperature zones. Figure 1 depicts the configurations of the PV/TW unit [23]. As a heat absorber, the PV panel is mounted on the south side of the space. In winter, two air slots are used for heating, while in summer, two more slots are meant for cooling. The summer air holes are closed and the winter air slots are opened to warm the air. The buoyancy effect causes room air to enter the air duct through the Down winter slots. This lowers the temperature of the sun cell in addition to producing thermal heat and energy. The temperature from the PV panel is extracted by the air inside the duct before it reaches the space. In contrast, the behavior is the reverse during the summer [14]. The goal of current work is to scrutinize the power output of the panel, its efficiency in terms of energy production, the air flow rate via the channel, and the effect of adding the Trombe wall on the building's energy. Additionally, over the course of a year, a parametric investigation of the impact of channel depth on a few functional aspects of the system was conducted.

Every modeling in the computer needs verification in order to be sure of the accuracy of the output obtained from that modeling. To confirm the outcomes produced by the programme, the experimental results of a solar panel in 18 days have been investigated with a fixed angle of 34 degrees in Cape Town, South Africa [24]. Figure 2 shows the accuracy of the modeling done with good experimental results and the error is less than 5%.

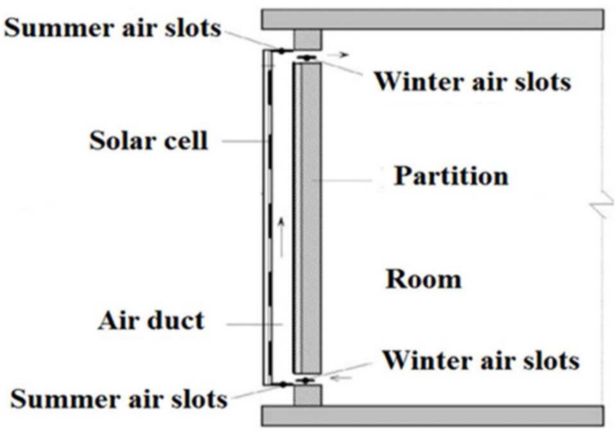

Fig. 1. Photovoltaic/Trombe wall [23].

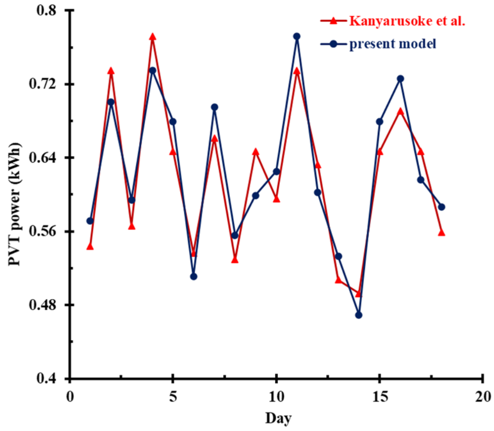

Fig. 2. Verification of the results obtained from the model and experimental data Africa [24].

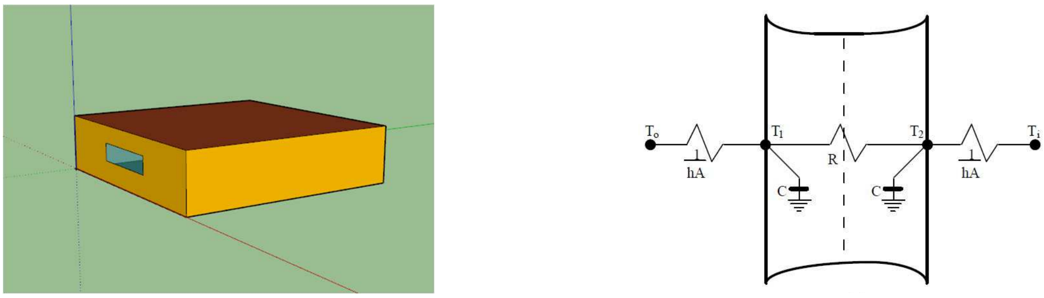

Fig. 3. (a) Schematic of the intended building (b) Heat transfer through the wall.

3. Materials and Methods

3.1. System modeling software

A framework for software simulation based on graphics called TRNSYS is implemented to simulate the behavior of transient systems. Though most modeling concentrates on assessing thermal and electrical energy performance, TRNSYS may also be used to represent other dynamic units like biological processes or traffic flow. TRNSYS consists of two components. The engine, sometimes referred to as the core, is the first component and is responsible for reading and processing the input file, solving the system repeatedly, determining convergence, and determining the variables of the energy system, such as thermophysical characteristics, matrix inversion, linear regressions, and crunching handles external data files. A vast library of components, each of which simulates the operation of a different system component, makes up TRNSYS' second section. About 150 models, from pumps to multifunctional structures, wind turbines to electrolyzer, meteorological data, and simple air conditioners utilized as cutting-edge machinery, are included in the standard library. Models are constructed so that users may add new features, change old ones, and expand the environment's capabilities.

3.2. Standard elements and weather data

TRNSYS has a library of extensive standard components to start modeling and simulation. Over the years, a number of other components and alternative libraries have been created by users. Links are found to some of the most well-known Thermal Energy Systems (TESS) experts. TRNSYS can read different types of weather data files. One of the most famous of them is the weather elements of TMY2 (Typical Metrological Year). This software also includes a method to create new components that are not available in the standard package. For more than thirty years, various applications have been supported by this simulation package.

3.3. Description of the simulated building

Figure 3(a) shows the schematic of a building, which is investigated in this study. In this building, for the heat transfer from the walls, it is founded on the heat transfer rules of conduction and convection. Two thermal resistance models can be imagined for the walls; Fig. 3(b) displays the initial model and Fig. 3(c) displays the second model. The building and related elements are modeled in TRNSYS software with applied assumptions. Table 1 provides a brief description of each component of the TRNSYS software that is used. (It should be noted that the relations used in this section are extracted from the relations of the TRNSYS library and the software uses these relations to solve and extract the outputs). As explained, Fig. 3(a) shows the schematic of a building investigated in this research. And Fig. 3(b) shows the initial thermal resistance model for the wall. And we also know that in this building heat transfer from the walls is based on the laws of conduction and convection heat transfer which is shown for a wall in Fig. 3(b).

4. Mathematical Modeling

The principle of conservation of energy is one of the most fundamental laws of nature. According to this theory, energy simply transforms from one shape to another and is never generated or destroyed. In fact, it shows the relationship between the system or the control volume of mass transfer, heat exchange and work with the surrounding environment. Energy has both amount and quality, according to the second rule of thermodynamics, and actual actions take place to lower the quality of energy.

Table 1. The elements used in TRNSYS software and their functions.

Element	Model	Function
Building	Type 56	It simulates a structure with several temperature zones. The input of this element type should be a simulated building and weather data file.
Integrator	Type 24	It is an integrator (a type of adder) and its use is when the user wants to measure the sum of a parameter in a period of time, for example, a month.
Trombe Wall	Type 36b	Trombe thermal energy storage wall is a wall with high thermal capacity to be coupled with the desired space. Absorbed solar energy can be transferred inside in two ways. One through radiation and the other through the heating of circulating air inside the room into the wall. Also, this wall models the heat loss of the wall.
Graph plotter	Type 65a	One type of output is a graph plotter and saves the data in a text file.
soil temperature	Type 77	This model models the soil temperature every hour and is used in buildings that are located on the ground floor and the floor is in contact with the soil.
Weather data	Type 15	It is a climate data element and it models the environmental conditions according to the desired climate that has been given to it in advance.
Text output	Type 25d	It is an output element that only displays data as text and does not output graphs.
solar panel	Type 50	It is used to model the solar panel.

4.1. Analysis of the process from the point of view of the first law of thermodynamics

For the purpose of the thermodynamic analysis of the process, each of its components is considered a control volume, and the following applications of the principles of conservation of mass and energy are made to it: For steady-state processes, neglecting changes in kinetic and the following is the expression for potential energy in terms of the principles of conservation of mass and energy [25]:

$$\sum \dot{m}_i = \sum \dot{m}_e \tag{1}$$

$$\sum_j \dot{Q}_j + \sum \dot{m}_i h_i = \sum_k \dot{W}_k + \sum \dot{m}_e h_e \tag{2}$$

The heat transfer to the control surface is denoted by $\dot{Q}_j$, the work done is denoted by $\dot{W}_k$, the mass flow rate is represented by $\dot{m}$, the enthalpy by h, and the flow in and out of the control volume is denoted by the indices *i* and *e*, respectively, in the aforementioned equations.

4.2. Process analysis from the perspective of the second law of thermodynamics

The examination of the procedure from the perspective of the first law was discussed in the preceding section. Actually, the first law quantitatively analyses thermodynamic processes. However, it doesn't offer details on the kind and quantity of energy. For this reason, in order to learn more about identifying the quality of energy supplies, it is necessary to use a new concept called exergy or accessibility.

Work cannot take place when a system in a process finds equilibrium with its surroundings since no spontaneous state change can happen at that point. Thus, a system has completed the maximum amount of reversible work when it achieves a condition of balance with its surroundings and is fully reversible. This means that the capacity to perform the greatest amount of work that the system is capable of is exergy in its initial condition.

The concepts of reversible work and exergy may be conveyed by drawing comparisons between an ideal system and a real system that have the same flows and input and output states. Reversible work is the least amount of work that can be supplied to the system or the greatest amount that can be gained from a certain combination of flows and heat transfer. The efficiency of the second law is determined by comparing the actual work to the maximal theoretical work. The efficiency of the second rule may also be applied to systems without shaft work, such as heat exchangers, by using the idea of exergy. In this instance, the ratio of exergies is utilized rather than the ratio of energies in the first rule when comparing the exergy production from one stream to the exergy received by another stream.

In contrast to energy, exergy is not always sustainable and can be destroyed. In fact, all of the exergy in a system that has achieved any kind of balance with its surroundings has been destroyed. In the absence of the effects of nuclear, magnetic, electric energy and surface tension, flow exergy is defined as follows [25]:

$$\dot{E} = \dot{E}_k + \dot{E}_p + \dot{E_{ph}} + \dot{E_{ch}} \tag{3}$$

Kinetic exergy [26]:

$$\dot{E}_k = \frac{1}{2}\dot{\text{m}}v^2 \tag{4}$$

Potential exergy [26]:

$$\dot{E}_p = \dot{\text{m}}gz \tag{5}$$

Physical exergy [26]:

$$\dot{E}_{ph} = \dot{\text{m}}\{(h - h_0) - T_0(s - s_0)\} \tag{6}$$

If the system has no chemical reaction, the amount of chemical exergy will be zero. Also, if kinetic exergy and potential are omitted, we will have only physical exergy from Eq. (6). In this case, the exergy balance equation will be as follows [25]:

$$\dot{E}_Q - \dot{W} = \sum \dot{m}_e e_e - \sum \dot{m}_i e_i + \dot{E}_D \tag{7}$$

The mass flow rate ($\dot{m}$), heat transfer rate ($\dot{Q}$) to the control volume, work rate ($\dot{W}$) performed by the control volume, input exergy rate ($\sum \dot{m}_i e_i$), and Output exergy rate ($\sum \dot{m}_e e_e$) are all represented by these numbers. The terms "exergy destruction rate" ($\dot{E}_D$) and "Exergy heat transfer rate" ($\dot{E}_Q$) have the following definitions [25]:

$$\dot{E}_Q = \sum \left(1 - \frac{T_0}{T}\right) \dot{Q} \tag{8}$$

In the above formula, T_0 is the ambient temperature.

4.3. Photovoltaic/thermal system modeling

The equation for the energy balance for every location along the collector's surface may be expressed as follows in order to represent the photovoltaic system [27, 28]:

$$\dot{Q}_{absorbed} = \dot{Q}_{loss.top.conv} + \dot{Q}_{loss.top.rad} + \dot{Q}_{loss.back} + \dot{Q}_u \tag{9}$$

where $\dot{Q}_{loss.top.conv}$, $\dot{Q}_{loss.top.rad}$, and $\dot{Q}_{loss.back}$ represent the heat lost by convection heat transfer and radiation energy loss from the top and back of the collector, respectively. Also, $\dot{Q}_u$ is the amount of energy added to the current by the collector. All the above sentences are calculated as follows [14, 24]:

$$\dot{Q}_{loss.top.conv} = \dot{h}_{outer} A(\bar{T}_{PVT} - T_{amb}) \tag{10}$$

$$\dot{Q}_{loss.top.rad} = \dot{h}_{rad} A(\bar{T}_{PVT} - T_{sky}) \tag{11}$$

$$\dot{Q}_{loss.back} = A \frac{\bar{T}_{absorbed} - \bar{T}_{inside}}{R_{Back}} \tag{12}$$

In Eq. (13), the absorbed energy can also be expressed as follows [28, 29]:

$$\dot{Q}_{absorbed} = \dot{G} A(\tau\alpha)(1 - \eta_{PV}) \tag{13}$$

where $\dot{G}$, A, $\tau\alpha$ and η represent the total radiation received from the sun, the panel area, the absorption coefficient for the sun panel and the solar panel's efficiency, respectively. Finally, the power of photovoltaic panels is as follows [27, 28]:

$$\dot{W}_{PVT} = \dot{G} A(\tau\alpha)\eta_{PV} \tag{14}$$

The exergy balance for the collector is suggested as follows [29]:

$$\begin{gathered} \sum \dot{E}x_{in} = \sum \dot{E}x_{out} + \sum \dot{E}x_D \\ \sum \dot{E}x_{sun} = \sum \dot{E}x_{thermal} + \sum \dot{E}x_{electrical} + \sum \dot{E}x_D \end{gathered} \tag{15}$$

As it is clear from Eq. (16), The exergy loss is equal to the input exergy from solar radiation less the thermal and electrical exergy, where [30] is the value of the sun's received exergy ($\dot{E}x_{sun}$):

$$\sum \dot{E}x_{sun} = \left[1 + \frac{1}{3}\left(\frac{T_0}{T_S}\right)^4 - \frac{4}{3}\left(\frac{T_0}{T_S}\right)\right] \dot{Q}_{Sun} \tag{16}$$

where T_S represents the temperature of the sun.

The total amount of energy, the rate of electrical energy generated, and the rate of energy squandered from the cell's surface to the environment equals the amount of energy that is received from the sun.

Two fundamental equations were given above in general. The energy and exergy analysis of PVT collectors is based on these two equations, from which more useful equations can ultimately be derived. Finding the ideal places in the functional and design characteristics to maximise energy efficiency has been the aim of this research.

4.4. Simple wall heat transfer

Equation (17) shows the differential equation of thermal balance, which is the basis of simulation [31]:

$$C_z \frac{dT_z}{dt} = \sum_{i=1}^{N_{sl}} \dot{Q}_i + \sum_{i=1}^{N_{surfaces}} h_i A_i (T_{si} - T_z) + \sum_{i=1}^{N_{zones}} \dot{m}_i C_p (T_{zi} - T_z) + \dot{m}_{inf} C_p (T_\infty - T_z) + \dot{Q}_{sys} \tag{17}$$

The relationship's left side corresponds to the variations in energy stored in the area under investigation, where T_z is the temperature of the target space and the coefficient C_z is obtained from Eq. (18) [31]:

$$C_z = \rho_{air} C_p \tag{18}$$

where ρ_{air} is equal to air density and C_p is air heat capacity.

In Eq. (17), on the right side, respectively, the total heat transfers of internal convective loads (related to elements inside the space, including lamps, electrical appliances, etc.) $\dot{Q}_i$, convective heat transfer with surfaces heat transfer coefficient displacement expressed in terms of (h_i) and difference the surface temperature of the walls (T_{si}) and the temperature of the space (T_z), the heat load resulting from the air mixing in areas with varying comfort temperatures measured by the air mass flow rate ($\dot{m}_i$) and the temperature differential between the areas ($T_{zi} - T_z$), the heat load resulting from the air piercing in terms of The temperature differential between the infiltrating air and the interior air ($T_\infty - T_z$), the mass flow rate of the infiltrating air ($\dot{m}_{inf}$), and the energy used by the air conditioning system for heating or cooling are all reported. The energy provided by the system is obtained from Eq. (19) [31]:

$$\dot{Q}_{sys} = \dot{m}_{sys} C_p (T_{sup} - T_z) \tag{19}$$

The following formulas can be used to calculate the heat transfer from the building's walls. Each of the equations expresses the exchange energy in the outer and inner half of the wall [31]:

$$C\frac{dT_1}{dt} = -q_o^{*} A + \frac{T_2 - T_1}{R} \tag{20}$$

$$C\frac{dT_2}{dt} = q_i^{*} A + \frac{T_1 - T_2}{R} \tag{21}$$

The left side of the relationship is equal to the energy changes stored inside the wall. The displacement heat transfer via convection from the outside and inner surfaces of the wall is represented by the values q_o^{*} and q_i^{*}, respectively, on the right side of the equation. The following formulae provide these values [31]:

$$q_o^{*} = h(T_o - T_1) \tag{22}$$

$$q_i^{*} = h(T_i - T_2) \tag{23}$$

Relations (24) and (25) obtain the C and R coefficients:

$$C = \frac{\rho c_p l A}{2} \tag{24}$$

$$R = \frac{l}{KA} \tag{25}$$

In all equations, heat transfer is in terms of [J] and temperatures are in terms of [K].

4.5. Heat transfer from the wall of heat storage

The complicated heat transport model presented in [32] can be reduced to a simpler version. Under the assumption that temperature and air density have a linear relationship, the air velocity on the wall may be computed as follows:

$$V = [\frac{2\text{gh}}{C_{ext}\left(\frac{A_g}{A_v}\right)^2 + C_{int}} \frac{T_a - T_{in}}{T_a}] \tag{26}$$

where the air passage's pressure decrease is $C_{ext}\left(\frac{A_g}{A_v}\right)^2 + C_{int}$. In addition, h, T_a, and T_{in}, respectively, represent the wall's height and the interior and exterior temperatures.

The air layer's thermal resistance as heat moves from the outside inward is equal to [33]:

$$R = \frac{A_m[\left(\frac{2h_c A_m}{\dot{m}C_p}\right)\left(\exp\left(-\frac{2h_c A_m}{\dot{m}C_p}\right) - 1\right) - 1]}{\dot{m}C_p(\exp\left(-\frac{2h_c A_m}{\dot{m}C_p}\right) - 1)}] \tag{27}$$

where $\dot{m}$ and h_c stand for the acronyms for the mass flow rate in the air channel and the air heat transfer coefficient, respectively, and A and C_p denote the area and heat transfer coefficient. The following formula determines the heat transfer coefficient depending on either turbulent or smooth flow:

$$Nu = 0.0158 Re^{0.8} \qquad \text{Laminar} \tag{28}$$

$$Nu = \frac{0.0606(\frac{R_e Pr\, d_h}{L})^{1.2}}{1+0.0909(\frac{R_e Pr d_h}{L})^{0.7} Pr^{0.17}} \qquad \text{Turbulent} \tag{29}$$

where the Reynolds and Prandtl numbers are represented by Re and Pr, respectively, and Nu is the Nusselt number. The above relationships are adapted from the TRNSYS software library, which is used to model the thermal storage wall [28].

The following reports provide information on the exergy efficiency of the solar panel and the wall that is linked to the room [34]:

$$\eta_{PV} = \frac{\dot{W}_{PV}}{\dot{E}x_{sun}} \tag{30}$$

$$\dot{E}_Q = \sum \left(1 - \frac{T_0}{T_{room}}\right) \dot{Q}_{to.room} \tag{31}$$

where η_{PV} is equal to the exergy efficiency of the solar panel and ($\dot{E}_Q$) is the room's thermal exergy value. Also, the panel's total efficiency, which is called η for short, is equal to [34]:

$$\eta = \eta_{th} + \eta_{ele} = \frac{\dot{W}_{PVT} + \dot{Q}_{PVT}}{\dot{E}x_{sun}} \tag{32}$$

where η_{th} is equal to [34]:

$$\eta_{th} = \frac{\dot{Q}_{PVT}}{\dot{E}x_{sun}} \tag{33}$$

Also, TRNSYS software has put the efficiency output in the definition of some PVT elements, so if we do not want to use the software to get the efficiency, the efficiency of the solar panel is equal to [29, 34]:

$$\eta_{pv} = \eta_{ref}(1 - \beta_{ref}(T_{pv} - T_{ref})) \tag{34}$$

where the subscript *ref* indicates the reference values.

5. Results and Discussions

This study's simulations are divided into three sections, which are respectively: simulation of a simple building with a thermal area; simulation of a solar panel; and finally, simulation of the proposed building, solar panel, and Trombe wall together.

5.1. Reviewed building model

The characteristics of the modeled building in the condition without the Trombe wall are shown in Table 2 and Fig. 4. The materials in the TRNbuilt plugin are modeled by TRNSYS software, and for this purpose, Google Sketchup software must be installed beforehand to be able to create a building model. Figure 3(a) displays the building schematic as it appears in the SketchUp software. This building is modeled at a height of 3 meters and on a land area of 144 square meters, and the goal is to find performance parameters for this building. The important point is that in using the TRNbuilt software, the materials and layers used are used according to Fig. 4, and if the materials are not available in the software library, it can be done by giving its specifications according to Table 2.

It should be noted that the use of insulation is optional, and the insulation layer can be removed. Because in heat transfer calculations by software, the use of insulation reduces heat transfer and declines the accuracy of temperature results. Table 3 depicts the final information about the desired thermal area. For instance, based on the materials utilized, the area's volume is 433 and its thermal capacity is determined to be 519.6.

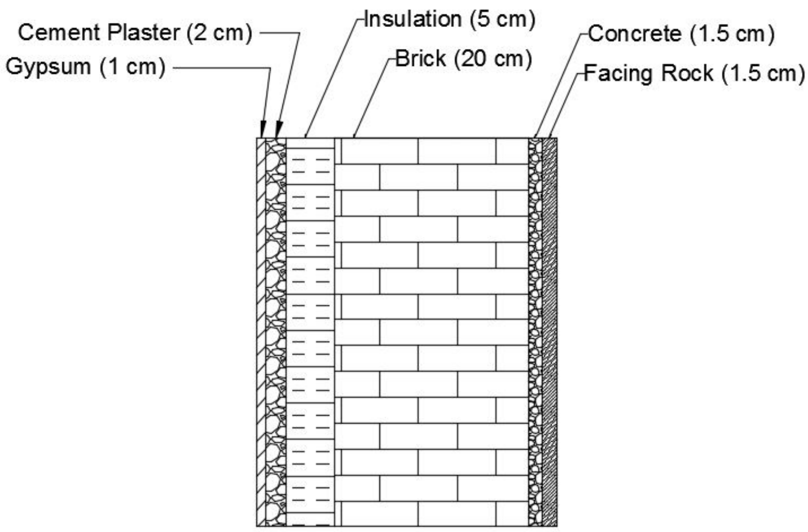

Fig. 4. Schematic of modeled building walls.

Table 2. Specifications of building walls.

The name of the layer	Conductivity K (W/K.m)	Density (Kg/m^3)	Specific heat capacity C_p (J/Kg.K)
Stone face	2.9	2590	860
Cement	1.75	1300	750
Brick	1.34	1900	900
Cement layer	0.72	1860	800

Table 3. Characteristics of different areas in the building.

Quantity	Amount	Unit
The volume of the thermal area	433	m^3
Heat capacity	519.6	kJ/K
Initial temperature	20	°C
The initial relative humidity of the area	50	%

5.2. Weather data

The sun and weather cycles are crucial for getting accurate results from the triple generation system simulation, as the input data from Kermanshah's weather conditions directly impacts the controllers' performance. Figures 5 and 6 display the ambient temperature and horizontal sun radiation for Kermanshah, respectively. In Fig. 5, the color green denotes the highest temperature at that period of the day, while the color light green denotes the lowest temperature. Also in Fig. 6, the orange colors show the amount of diffuse radiation, and the yellow color shows the total radiation. The Standard Typical Metrological Year (TMY2) format data file containing this data was derived from Type 109 [29, 34]. Also, the data was used from Meteonorm software, which uses the Kermanshah station to obtain meteorological information. To get climatic data, the average of the years 2000–2019 has also been used. A closer look at these data highlights how crucial it is that solar radiation not exceeds 220 kW/m^2. Furthermore, the summertime temperature has risen from -10 degrees Celsius to 41 degrees Celsius. The photovoltaic system has a lot of room to increase its performance, as these Figs demonstrate.

In this investigation, the utilization of input data derived from the weather conditions in Kermanshah directly influences the efficacy of the controllers. Figures 5 and 6 depict the ambient temperature and solar radiation on the horizontal plane for Kermanshah, respectively. Additionally, pertinent initial parameters include a temperature of 20 °C, a relative humidity of 50%, and a heat capacity of 519.6 kJ/K, based on the materials employed. Furthermore, the temperature range extends from -10 °C in winter to 41 °C in summer. These findings underscore the significant potential for enhancing system performance within the PV/TW setup.

According to the modelling done and the relationships in the fourth section, Fig. 7 illustrates how the solar panel's output power might be expressed for various months. According to this Fig, which can be calculated from Eq. (12) and is measured as an integral over a month, it is shown in Fig. 7. Production capacity in the early months of the year is lower than in the hot months owing to radiation. Also, due to the fact that the radiation angle has an effect on the amount of production power, this importance can be seen in the production power of the hot months within the year. The greatest output power, which happens in August–September, is 207 kW.

Another crucial aspect worth verifying is the solar panel's energy efficiency and output across different seasons, as illustrated in Figs. 8 and 9. It is noteworthy that the exergy performance of solar panels frequently surpasses their energy efficiency. The peak efficiency values are 22% for energy efficiency and 20% for exergy efficiency. Additionally, it is imperative to consider that solar panel efficiency is influenced by temperature, with efficiency often increasing during colder months of the year.

Fig. 5. The annual temperature changes of Kermanshah obtained from Meteonorm software.

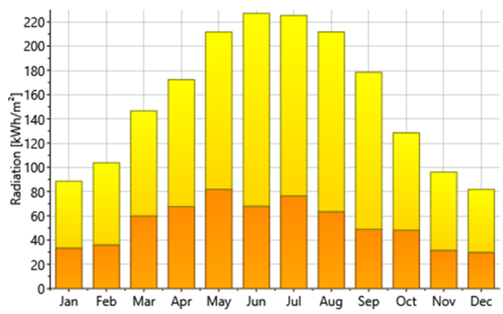

Fig. 6. Kermanshah radiation changes obtained from Meteonorm software.

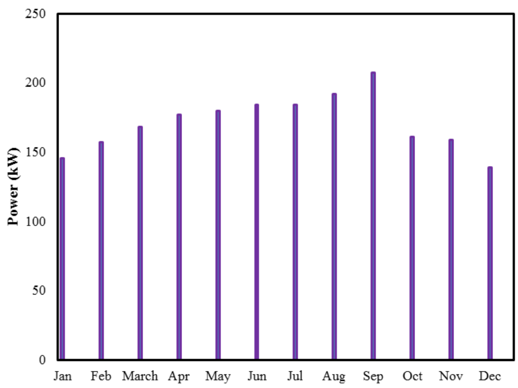

Fig. 7. Variations in the amount of power generated by solar panels throughout the year.

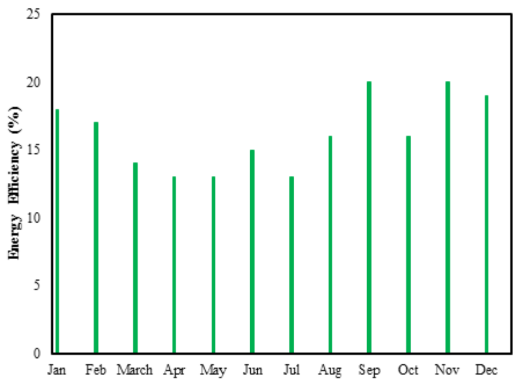

Fig. 8. The energy efficiency of solar panels varies according to the month of the year.

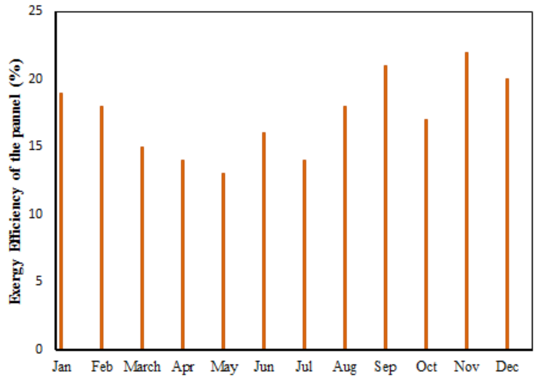

Fig. 9. variations in the exergy efficiency of solar panels throughout the year.

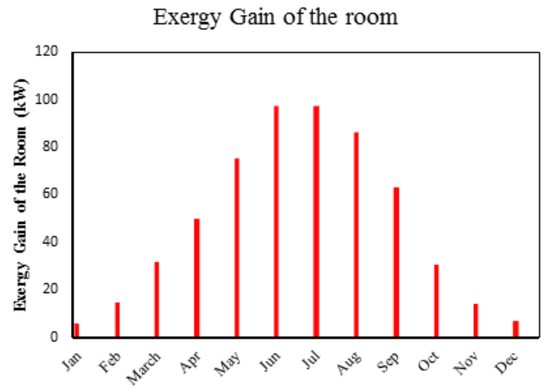

Fig. 10. Variations in the thermal area's exergy received throughout the year.

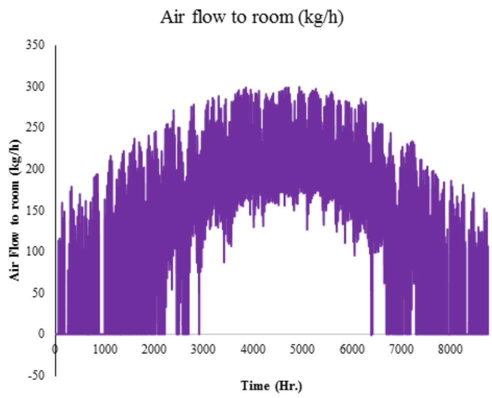

Fig. 11. Changes in the flow of air passing through the channel at different times of the year.

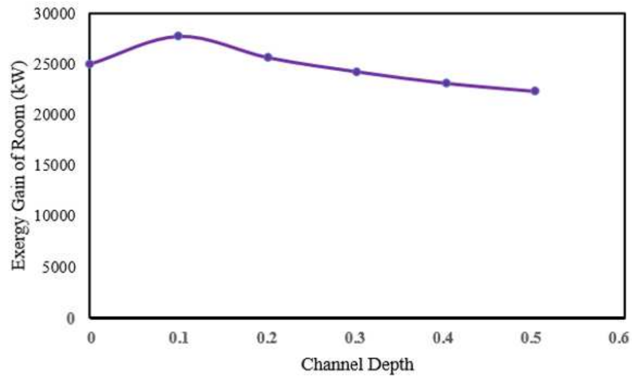

Fig. 12. Impact of the depth of the Trombe wall channel on the received exergy of the desired space.

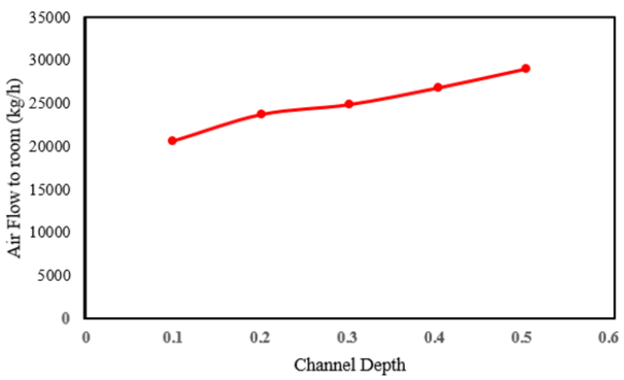

Fig. 13. Impact of the depth of the Trombe wall channel on air flow through it.

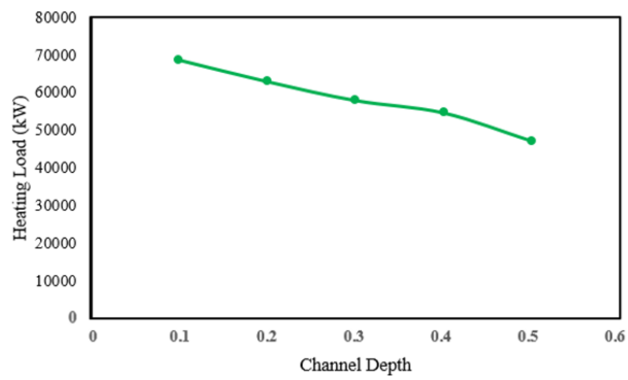

Fig. 14. The efficacy of the depth of the Trombe wall channel on the annual heating load.

Figure 10 illustrates how the amount of exergy in a room increases as radiation levels rise during the course of the year. Considering this Fig, in June and July, 100 kilowatts enter the exergy room through radiation. The air moving through the Trombe wall is one-way heat that is transferred from the wall into the space, and in Fig. 11, these flow rate variations throughout the year are displayed.

Figure 12 illustrates how the channel depth affects the room's received exergy. According to this Fig, it increases at first and subsequently diminishes as the channel's depth increases, and it rises to a maximum value of 27740 kW during a year. The important thing to note is that because of the summertime rise in flow rate and the room's drop in temperature caused by the Trombe wall, the received exergy does not change much.

The flow through the channel is seen in Fig. 13 as the channel depth increases. According to this Figure, It is evident that when the channel's depth increases, the passage of the flow rate through the channel is also increasing, and its highest annual value occurs at a depth of 0.5 meters, which is equal to 29,000 kg/h.

Another useful parameter that has been studied is the efficacy of increasing the channel's depth on the needed heating load during the winter which is shown in Fig. 14. Considering that the speed at which air passes through the channel augments with the rise in the depth of the channel, it can be predicted that the required heating load will also decrease, and by reducing the depth of duct, we will have the highest heating load (annually), which is equal to 68676 kW.

Figure 15 depicts the efficacy of the duct depth on the wall efficiency, PV, total, and total second law. The system's behavior is influenced by two factors: buoyancy forces and frictional losses. Both of them peak at the channel's lowest depth, however frictional losses outweigh buoyancy forces. Flotation forces take over as the channel gets deeper. The hydraulic diameter has the most impact on buoyancy forces and friction losses; however, there are several other factors as well. Both of them reduce quickly as the channel's depth grows, and when the depth increases yet further, they eventually approach constant values. This causes the system's efficiency at low channel depths to rapidly fluctuate and approach constant values in terms of parameters. Consequently, the maximum mass flow rate and thermal efficiency determine the ideal channel depth. As may be observed, the channel's depth of 5 to 15 cm is ideal for maximizing thermal efficiency. Since the heat transmitted from the PV to other components determines the PV temperature, an increase in channel depth causes to a drop in PV temperature and intensification in electrical efficiency. In actuality, the mass flow rate rises along with the channel's depth, but the exit air temperature falls. The prevalent circumstances determine how the second law of thermal efficiency changes. It is evident that thermal efficiency and the second law's thermal performance curve are comparable.

Finally, the investigated building has been modeled for the climate of Kermanshah by using these types of walls, and the effect of cooling and heating loads on it has been observed. Figs 16 and 17 depict the heating and cooling requirements for the structure under consideration in the scenarios with and without the Trombe wall, respectively. According to Fig. 16, the building needs an average heating demand of 8000 kJ/h and a maximum cooling demand of 8000 kJ/h without Trombe wall installation. Fig. 17 shows that after integrating PV-TW into the walls of the building, the house's requirements for heating and cooling drop dramatically (by around 3%). Using a Trombe wall lowers the heating and cooling loads, which in turn lowers the size of system components, which saves money.

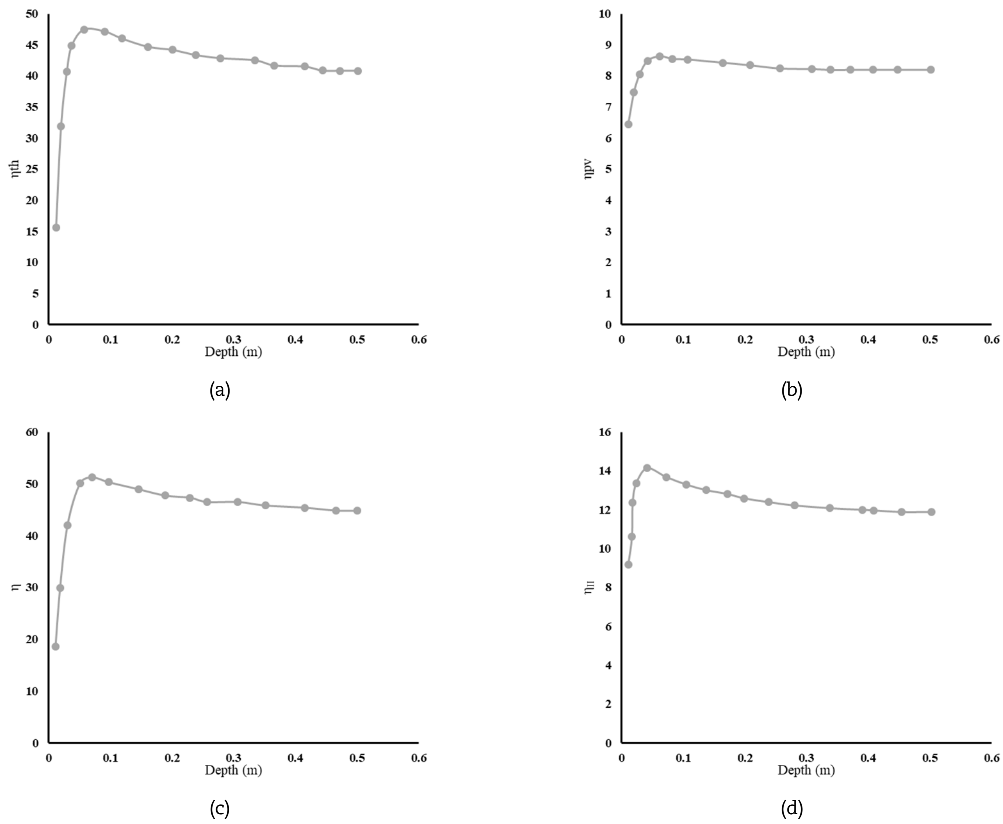

Fig. 15. Efficacy of channel depth on (a) wall efficiency, (b) PV efficiency, (c) total efficiency, (d) total second law efficiency.

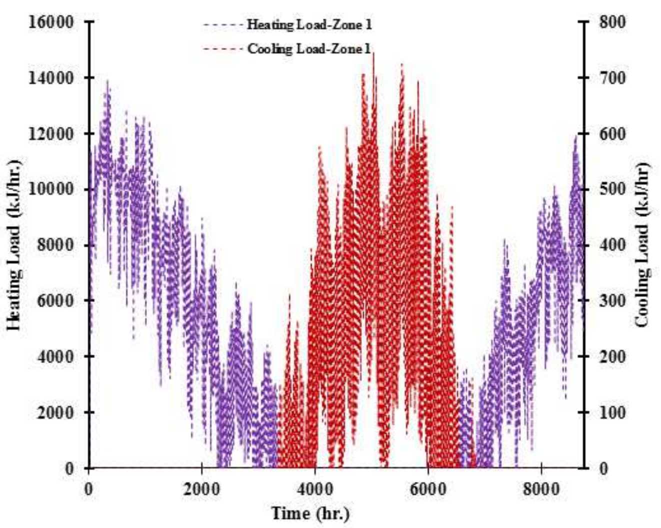

Fig. 16. The anticipated loads for the building in the absence of a Trombe wall.

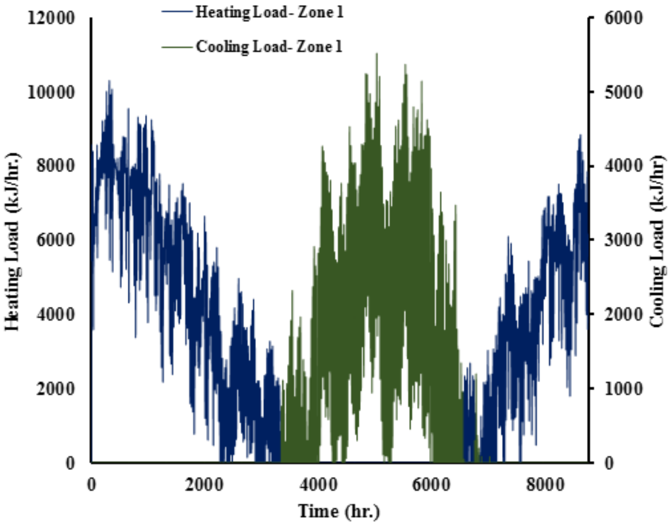

Fig. 17. The building's anticipated cooling and heating loads with the Trombe wall.

6. Conclusion

This study aimed to reduce building energy consumption through the implementation of photovoltaic Trombe walls, with an additional focus on identifying irreversible energy sources through energy analysis. The modeling was conducted using TRNSYS software, utilizing weather data from Kermanshah. The key findings of this study are as follows:

- The solar panel exhibits maximum power production of 207 kilowatts, occurring in July.
- Solar cell temperature significantly influences panel performance, with improved efficiency observed in cooler months with high radiation, such as August and September.
- Exergy efficiency surpasses energy efficiency due to the lower exergy received by the panels relative to energy received.
- Maximum exergy efficiency is achieved with a Trombe wall depth of 10 cm.
- Utilizing a Trombe wall reduces building heating and cooling loads by 3%, with optimal exergy efficiency also achieved at a 10 cm wall depth. Additionally, increasing channel depth reduces heating requirements and enhances channel flow.
- December sees peak energy efficiency due to intense solar panel exposure.
- The implementation of a Trombe wall decreases building heating and cooling demands by 3%.
- Increasing channel depth results in buoyancy forces becoming predominant, with hydraulic diameter exerting significant influence on buoyancy forces and friction losses. Buoyancy forces and frictional losses decrease rapidly as channel depth increases, eventually stabilizing at constant values.

Future research endeavors may involve integrating TRNSYS outputs with ANSYS FLUENT software and incorporating a paraffin layer within the system to further enhance performance.

Author Contributions

All authors planned the scheme, developed the mathematical modeling and examined the theory validation. The manuscript was written through the contribution by all authors. All authors discussed the results, reviewed, and approved the final version of the manuscript

Acknowledgments

The authors would like to thank the reviewers for their careful reading of the paper and their helpful comments.

Conflict of Interest

The authors declared no potential conflicts of interest concerning the research, authorship, and publication of this article.

Funding

The authors received no financial support for the research, authorship, and publication of this article.

Data Availability Statements

The datasets generated and/or analyzed during the current study are available from the corresponding author on reasonable request.

References

[1] Mahmood Ibrahim, A., Ibraheem, R.R., Bakr Weli, R., Energy saving in batteries using the photovoltaic system, *Al-Kitab Journal for Pure Sciences*, 4(1), 2023, 78–94.

[2] Ahmed, O.K., A numerical and experimental investigation for a triangular storage collector, *Solar Energy*, 171, 2018, 884-892.

[3] Elmariami, A., El-Osta, W., Nassar, Y., Khalifa, Y., Elfleet, M., Life cycle assessment of 20 MW wind farm in Libya, *Applied Solar Energy*, 59(1), 2023, 64-78.

[4] Ibrahim, A.K., Algburi, S., Ahmed, O.K., Enhancement of the performance of the PV Trombe Wall: A short review, *Cleaner Engineering and Technology*, 14, 2023, 100652.
[5] Gholamian, E., Ahmadi, P., Hanafizadeh, P., Ashjaee, M., Dynamic feasibility assessment and 3E analysis of a smart building energy system integrated with hybrid photovoltaic-thermal panels and energy storage, *Sustainable Energy Technologies and Assessments*, 42, 2020, 100835.
[6] BP, 2022. BP Statistical review of world energy 2022, (71st edition) [Online]. Available. https://www.bp.com/content/dam/bp/business-sites/en/global/corporate/pdfs/energy economics/statistical-review/bp-stats-review-2022-full-report.pdf.
[7] Xiao, Y., Zhang, T., Liu, Z., Fukuda, H., Thermal performance study of low-e glass Trombe wall assisted with the temperature-controlled ventilation system in Hot-Summer/Cold-Winter Zone of China, *Case Studies in Thermal Engineering*, 45, 2023, 102882.
[8] Ahmed, O.K., Hamada, K.I., Salih, A.M., Daoud, R.W., A state of the art review of PV-Trombe wall system: design and applications, *Environmental Progress & Sustainable Energy*, 39, 2020, e13370.
[9] Rezaei, M., Atikol, U., Özdenefe, M., Promotion of Trombe wall through demand-side management, *Solar Energy*, 206, 2020, 216-227.
[10] Zhang, H., Shu, H., A comprehensive evaluation on energy, economic and environmental performance of the Trombe wall during the heating season, *Journal of Thermal Science*, 28, 2019, 1141-1149.
[11] Hernández-López, I., Xamán, J., Chávez, Y., Hernández-Pérez, I., Alvarado-Juárez, R., Thermal energy storage and losses in a room-Trombe wall system located in Mexico, *Energy*, 109, 2016, 512-524.
[12] Abbas, F.F., Aziz, S.A., The impact of air gap width on the free thermal load in the trombe wall contains a phase change material, *Al-Kitab Journal for Pure Sciences*, 2(2), 2022, 264–275.
[13] Chen, B., Zhao, J., Chen, C., Zhuang, Z., *Experimental investigation of natural convection in Trombe wall systems*, Energy Systems Laboratory, 2006.
[14] Chen, B., Chen, H.J., Meng, S.R., Chen, X., Sun, P., Ding, Y.H., The effect of Trombe wall on indoor humid climate in Dalian, China, *Renewable Energy*, 31(3), 2006, 333-343.
[15] Shen, J., Lassue, S., Zalewski, L., Huang, D., Numerical study on thermal behavior of classical or composite Trombe solar walls, *Energy and Buildings*, 39(8), 2007, 962-974.
[16] Chen, W., Liu, W., Numerical analysis of heat transfer in a passive solar composite wall with porous absorber, *Applied Thermal Engineering*, 28(11-12), 2008, 1251-1258.
[17] Nwachukwu, N.P., Okonkwo, W.I., Effect of an Absorptive Coating on Solar Energy Storage in a Thrombe wall system, *Energy and Buildings*, 40(3), 2008, 371-374.
[18] Irshad, K., Habib, K., Thirumalaiswamy, N., Performance evaluation of PV-Trombe wall for sustainable building development, *Procedia CIRP*, 26, 2015, 624-629.
[19] Algburi, S., Ahmed, O.K., Abdullah, A.A., Atallah, F.S., Comparative assessment of PV/Trombe wall performance: Compound influence of paraffin wax and reflective mirrors, *Results in Engineering*, 20, 2023, 101433.
[20] Kalair, A.R., Seyedmahmoudian, M., Stojcevski, A., Mekhilef, S., Abas, N., Koh, K., Thermal comfort analysis of a trombe wall integrated multi-energy nanogrid building, *Journal of Building Engineering*, 78, 2023, 107623.
[21] Sheikholeslami, M., Al-Hussein, H.R.A., Modification of heat storage system involving Trombe wall in existence of paraffin enhanced with nanoparticles, *Journal of Energy Storage*, 58, 2023, 106419.
[22] Sheikholeslami, M., Al-Hussein, H.R.A., Analyzing efficiency of solar heat storage unit within a building including trombe wall equipped with phase change material in existence of fins, *Journal of Building Engineering*, 71, 2023, 106406.
[23] Ibrahim, A.K., Ahmed, O.K., Algburi, S., Optimum angle of reflective mirrors integrated on PV/Trombe wall: An experimental assessment, *Energy Reports*, 10, 2023, 591-603.
[24] Kanyarusoke, K., Gryzagoridis, J., Oliver, G., Validation of TRNSYS modelling for a fixed slope photovoltaic panel, *Turkish Journal of Electrical Engineering and Computer Sciences*, 24(6), 2016, 4763-4772.
[25] Moran, M.J., Shapiro, H.N., Boettner, D.D., Bailey, M.B., *Fundamentals of engineering thermodynamics*, John Wiley & Sons, 2018.
[26] Bejan, A., Tsatsaronis, G., Moran, M., *Thermal Design and Optimization*, John Wiley and Sons, New York, 1996.
[27] Behzadi, A., Gholamian, E., Ahmadi, P., Habibollahzade, A., Ashjaee, M., Energy, exergy and exergoeconomic (3E) analyses and multi-objective optimization of a solar and geothermal based integrated energy system, *Applied Thermal Engineering*, 143, 2018, 1011-1022.
[28] Klein, S.A., *TRNSYS-A transient system simulation program*, University of Wisconsin-Madison, Engineering Experiment Station Report, 38-12, 1998.
[29] Duan, S., Jing, C., Zhao, Z., Energy and exergy analysis of different Trombe walls., *Energy and Buildings*, 126, 2016, 517-523.
[30] Naserabad, S.N., Rafee, R., Saedodin, S., Ahmadi, P., Multi-objective optimization of a building integrated energy system and assessing the effectiveness of supportive energy policies in Iran, *Sustainable Energy Technologies and Assessments*, 47, 2021, 101343.
[31] Storey, A.A., Ramirez, J.M., Quiroz, D., Burley, D.V., Addison, D.J., Walter, R., ..., Matisoo-Smith, E.A., Radiocarbon and DNA evidence for a pre-Columbian introduction of Polynesian chickens to Chile, *Proceedings of the National Academy of Sciences*, 104(25), 2007, 10335-10339.
[32] Zhu, N., Li, S., Hu, P., Lei, F., Deng, R., Numerical investigations on performance of phase change material Trombe wall in building, *Energy*, 187, 2019, 116057.
[33] Abbassi, F., Dimassi, N., Dehmani, L., Energetic study of a Trombe wall system under different Tunisian building configurations, *Energy and Buildings*, 80, 2014, 302-308.
[34] Compton, M., Rezaie, B., Investigating steam turbine feasibility to improve the sustainability of a biomass boiler using TRNSYS, *Sustainable Cities and Society*, 43, 2018, 86-94.

ORCID iD

E. Azizi https://orcid.org/0009-0002-5051-8062
H. Safarzadeh https://orcid.org/0000-0002-1493-3851

How to cite this article: Azizi E., Safarzadeh H. Numerical assessment of solar system including trombe wall and photovoltaic module, *J. Appl. Comput. Mech.*, 11(3), 2025, 742-753. https://doi.org/10.22055/jacm.2024.47775.4785